Theoretical Modeling on Chemical Composition and Mechanical Properties of Well Cement under Carbonation Reactions

Linfei Li[a], Mija H. Hubler[a], Yunping Xi[a,*]

[a] University of Colorado, Department of Civil and Environmental Engineering, Boulder, CO 80309, USA
[*] Corresponding author.
E-mail address: yunping.xi@colorado.edu (Xi, Y.).

Abstract

This paper presents theoretical models of the phase transformation and the change of mechanical properties of oil well cement due to underground carbonation reactions. Application of oil well cement has become common practice in CO_2 underground storage formations. However, the CO_2 stored underground may leak through damaged well cement, and it can cause carbonation reactions which may significantly decrease the mechanical properties of well cement. Extensive research has been conducted by using experimental methods in laboratories to characterize the carbonation reactions of cement underground. However, no theoretical formulations have been developed considering the mechanical properties change due to the carbonation effect. In this paper, the CO_2 profile was predicted first by the error function solution of a 1D CO_2 diffusion equation and further the carbonation reaction rate was calculated. The phase transformation of well cement due to carbonation were then analyzed by using a stoichiometric model. After that, the changes of mechanical properties of well cement were modeled using a two-phase generalized self-consistent model at different scales. Specifically, the decrease of the elastic modulus of well cement during the carbonation process was used as an example application of the model. Finally, the modeling result was validated with published experimental results.

Keywords: Carbonation, Diffusion, Oil Well Cement, $Ca(OH)_2$, Elastic Moduli

1 Introduction

With the development of technology and civilization, a large amount of raw resource has been used without decent recycle of detrimental substances in the past 50 years [1]. As the consequences, the living environment of mankind is threatened in various aspects. In recent years, more and more environmental issues have been reported by researchers, such as climate change, acid rain, ozone depletion, etc. [2,3]. As one of the most severe environmental problem among them, the climate change has been addressed with a great effort [1,4,5,6]. In order to control climate change and the amount of greenhouse gas emitted to the atmosphere, CO_2 emission, which is the main compositions of greenhouse gas, has to be reduced tremendously around the world. This reduction can be done by various techniques, and long-term storage of CO_2 is one of them [1]. Off-shore and in-shore storage such as deep saline geological units, as well as mineral sequestration are the three available techniques for CO_2 storage. Under consideration of technical difficulty level and safety issues, geological storage became the most advanced technology to be used for CO_2 storage and many large industrial scale and pilot projects have successfully transported CO_2 into underground reservoirs [1]. In the last 20 years, more than 100 projects have been successfully completed to inject CO_2 into underground reservoirs [1]. Fig. 1 shows the side view of a borehole system. The steel pipe is installed first, then the well cement is injected through the steel pipe and hardens around the outside of it. The cementing process of the wellbore is very important to keep the injected CO_2 underground, and cementing can be split into two types: primary cementing and remedial cementing. Primary cementing refers to the placement of the cement underground into the annular space to provide zonal isolation. Remedial cementing refers to the repair of the primary cement after the wellbore has been constructed, which includes the processes of squeezing cementing and plugging cementing [7]. Remedial cementing is expensive. Therefore, thoroughly

planning and designing primary cementing is necessary and economical. Long after injection, CO_2 can move upward or sideways due to the unbalanced pressure in the subsurface [4]. To safely keep the injected CO_2 underground, the long-term mechanical properties of cement in the borehole system need to be well understood. Any significant deterioration in mechanical properties of the well cement may result in potential leakage of the CO_2. So, the durability of well cement has become a center of attention in the research community [5].

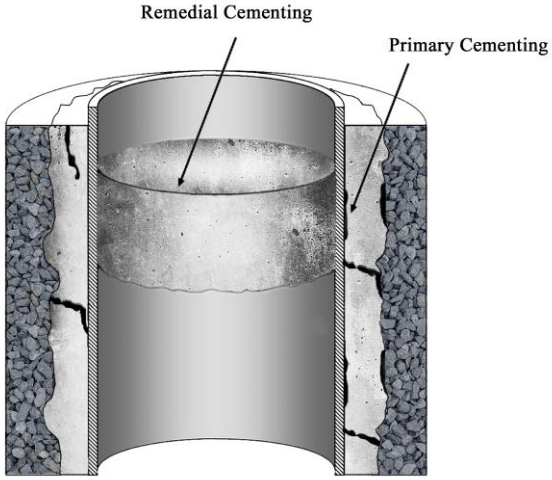

Figure 1. Primary cementing and remedial cementing

Carbon dioxide either from the atmosphere or from underground storage can react with the hydration products in cementitious material [8], which are called carbonation reactions Due to the carbonation reactions, both the mechanical properties and durability of cementitious materials can be potentially affected to different extents. In the past several decades, a lot of research has focused on understanding the mechanism of carbonations on concrete structures above the ground and trying to mitigate the effect of carbonations. Bertolini et al. [6] mentioned in their research that the carbonation reactions can reduce the pH value of the pore solution, which can lower the depassivation threshold of the reinforcing steel and further encourage the corrosion of steel casing [9]. Besides decreasing the pH value in the cementitious material, the chemical compositions can also be changed due to the invasion of CO_2 [10]. Relevant experimental studies have been

conducted to mainly measure the 'carbonation front', which is one of the most important parameters to define the carbonation depth [11,12] in the cementitious material. Thermogravimetric analysis (TGA) has been introduced to analyze the effect of carbonation reactions on the cementitious material, where the change of chemical compositions of cement can be captured [13]. In addition to the experimental studies, models have been developed to simulate the carbonation effects in cementitious material under different conditions [14-18]. It can be seen from these modeling that although different environmental conditions have been included in the model, an important part of the carbonation reactions, called the wet carbonation has been neglected, which is important specifically for the underground environment.

From previous experimental research, it has been concluded that carbonation reactions can be divided into two types: dry carbonation and wet carbonation (or carbonation stage and dissolution stage) [19-23]. The carbonation reactions of well cement can be generally expressed using the chemical equations 1-7 and Fig. 2:

$$CO_2 + H_2O \leftrightarrow H_2CO_3 \leftrightarrow H^+ + HCO_3^- \leftrightarrow 2H^+ + CO_3^{2-} \quad (1)$$

$$Ca(OH)_2 + 2H^+ + CO_3^{2-} \rightarrow CaCO_3 + 2H_2O \quad (2)$$

$$Ca(OH)_2 + H^+ + HCO_3^- \rightarrow CaCO_3 + 2H_2O \quad (3)$$

$$C-S-H + 2H^+ + CO_3^{2-} \rightarrow CaCO_3 + SiO_xOH_x \quad (4)$$

$$C-S-H + H^+ + HCO_3^- \rightarrow CaCO_3 + SiO_xOH_x \quad (5)$$

$$CO_2 + H_2O + CaCO_3 \leftrightarrow Ca^{2+} + 2HCO_3^- \quad (6)$$

$$2H^+ + CaCO_3 \leftrightarrow CO_2 + Ca^{2+} + H_2O \quad (7)$$

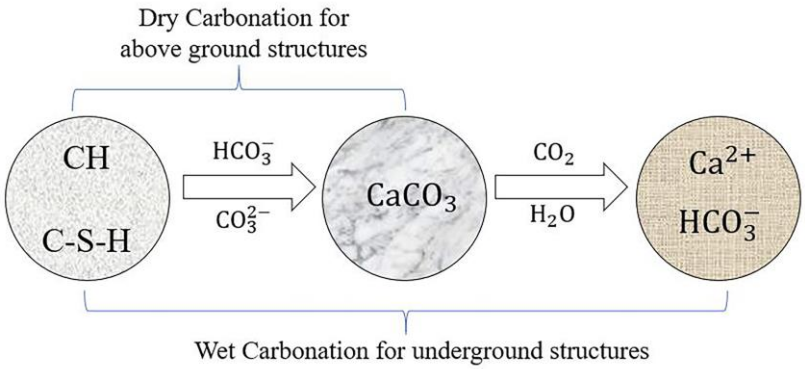

Figure 2. Phase transformations during the carbonation reaction

The chemical equations show the entire progression of the carbonation reactions. In equation 1, the CO_2 reacts with water to produce carbonic acid and bicarbonic acid [24]. In the next step, equations 2 to 5, the acid reacts with the calcium hydroxide first to generate the calcium carbonate, and then, the calcium silicate hydrate (C-S-H) gel (a hydration product of well cement) reacts with the acid to form the amorphous silica gel and calcium carbonate. During this step, the stiffness of calcium carbonate is high, and it can increase the strength of the cement, while the amorphous silica can decrease the permeability. This step is called "dry carbonation", which happens in regular Portland cement concrete above ground structures. If the cement continuously encounters brine, which is common in the underground environment, the reactions go through the entire process from equations 1 through 7. At the end of the reactions (equations 6 and 7), the calcium carbonate content decreases, and the strength of the cement decreases as well. This is called "wet carbonation". It is important to note that the results of the two carbonation processes are totally different. For dry carbonation, the cement is stronger after the carbonation reactions. On the other hand, the cement is weaker from the wet carbonation. So, the outcome of the wet carbonation is more harmful to the mechanical properties of well cement underground than the dry carbonation. The rate of carbonation reactions becomes an important factor in the mechanical deterioration process of well cement [25,26]. Many influential factors have been considered to affect the rate of

carbonation reaction: relative humidity, water to cement ratio, initial CO_2 content of the environment, types of cement used, temperature, pressure, etc. In order to study the effect of these factors, researchers have conducted experimental tests and developed mathematical models to predict the influence of each factor [27-34]. From their results, one can conclude that with the increase of temperature, the rate of carbonation reactions is increased. The influence of pressure has also been considered in [27] showing that the higher pressure could help to push the CO_2 gas farther into the cement. As the result, the carbonation reaction could start at deeper depths of the cement annulus. Since the pressure and temperature are much higher in the underground environment than above the ground [35,36], it is necessary to focus on the carbonation reaction in this study. In addition, the water-to-cement ratio is another important factor. As shown in previous research, with a higher water-to-cement ratio, the carbonation reactions are faster [37].

Based on the literature review above, one can conclude that the CO_2 stored underground may leak through damaged well cement, and it can cause carbonation reactions which may significantly decrease the mechanical properties of well cement. Although a lot of experimental research was conducted, there is no systematic modeling work that focuses on both the changes of chemical compositions and mechanical properties of the well cement use in underground structures due to the carbonation reactions. The wet carbonation, which is emphasized here, is only seen in past experimental studies. There is no modeling work currently considering the mechanical properties effect of wet carbonation on cementitious material used in underground projects. At the macrostructure level, the reaction rate is indirectly defined by the carbonation depth instead of the degree of carbonation, implying that larger carbonation depth in a structure are an indication of a higher reaction rate. However, the degree of carbonation is a better indicator than the carbonation depth because it directly shows the extent of the phase transformations that have occurred in the

cementitious material. Hence, it is necessary to build a systematic theoretical model to characterize the carbonation reaction processes in terms of the associated phase transformation, reaction rate and their effects on the mechanical properties of well cement. In the next section, the initial volume fraction of well cement due to the hydration process is simulated by using stoichiometric model. Section 3 shows the phase transformations in the well cement due to the carbonation reaction by using the same stoichiometric model. In section 4, the two-phase general self-consistent (GSC) model is applied. As a numerical example, the modulus of elasticity of well cement is modeled. The validation work of the model is conducted in section 5. Consistent results are obtained between the model prediction and previous experimental results. This theoretical analysis is the first step towards realistic estimation of the long-term performance of wellbore system for underground CO_2 storage reservoir.

2 Initial Volume Fractions of Constituents after Hydration Process of Well Cement

To evaluate the changes of chemical composition and mechanical properties of well cement during the carbonation reactions, the initial conditions of the cement before the carbonation reactions start must be understood. These initial values depend on the degree of hydration of cement. To simplify the calculation with nearly no effect on the long-term model accuracy, it can be assumed that the carbonation reactions start right away after the hydration reactions of cement are completed. Therefore, the initial volume fractions of the hydration products in the cement paste can be calculated based on the total hydration of cement.

According to the API 10A Standard [38], oil well cement can be categorized in six classes: A, B, C, D, G, and H, each divided into three grades: ordinary (O), moderate sulfate-resistant (MSR), and high sulfate-resistant (HSR). Classes A, B, and C are similar to type I, II, and III cements in the ASTM standard C150 and ASTM C465 [39,40]. Class D cement is used for moderately high

153 temperatures and pressures under MSR and HSR grades. The definitions of Class G and Class H
154 cements are similar in the API standard. Both can be used as a basic well cement casing and work
155 in MSR and HSR grades except the size of Class G cement particles is finer than that of Class H
156 cement. According to data from the Society of Petroleum Engineers (SPE), approximately 80% of
157 the projects in the U.S. adopt Class H and G cement and greater than 95% of the projects in the
158 rest of the world use Class G cement. Class G and H cements have better performance under high
159 temperature and high pressure than the other four classes. In addition, other special cements are
160 used for oil well cementing although they are not very common, including: Pozzolanic-Portland
161 Cement, Gypsum Cement, Microfine Cement, Expanding Cements, Calcium Aluminate Cement,
162 ThermaLockTM, Latex Cement, Resin or Plastic Cements, Sorel Cement, and EverCRETETM
163 CO2, etc. [41]. Compared with ordinary cement used for the structures above the ground, well
164 cement has unique advantages for underground projects: high fluidity and relatively low thermal
165 contraction. However, in order to achieve the high fluidity, this specific material sacrifices the
166 mechanical properties and durability to some extent. From previous work, the lower strength of
167 well cement did not considerably affect the sealing process of CO_2 gas in the wellbore system [4].
168 Class G cement is selected as the well cement used in the modeling work based on the common
169 application around the world. The water-to-cement (w/c) ratio is equal to 0.44 (API 10A standard).
170 The mineral compositions of cement powder are shown in Table 1 [42]. The hydration equations
171 are shown below:

172 $$C_3S + 5.3H \rightarrow 0.5C_{3.4}S_2H_8 + 1.3CH \quad (8)$$

173 $$C_2S + 4.3H \rightarrow 0.5C_{3.4}S_2H_8 + 0.3CH \quad (9)$$

174 $$C_4AF + 2CH + 10H \rightarrow 2C_3(A,F)H_6 \text{ (Hydrogarnet)} \quad (10)$$

175 $$C_3A + 3CSH_2 + 26H \rightarrow C_6AS_3H_{32} \text{ Ettringite (AFt)} \quad (11)$$

$$C_3A + 0.5C_6AS_3H_{32} + 2H \rightarrow 1.5C_4ASH_{12}\ \text{Monosulfate (AFm)} \quad (12)$$

$$C_3A + CH + 12H \rightarrow C_4AH_{13}\ \text{Calcium aluminate hydrate} \quad (13)$$

Table 1 Chemical composition of Class G cement [38]

Mineral Composition	C_3S	C_2S	C_3A	C_4AF
% by mass	56	25.7	2	16.3

The hydration products and the total volume are expressed in equations 14 and 15 [32].

$$V_{total} = V_c^0 + V_w^0 \quad (14)$$

$$V_{total} = V_w(t) + V_{ck}^i(t) + V_{CSH}(t) + V_{CH}(t) + V_{AL}(t) + V_{cp}(t) = 1 \quad (15)$$

To calculate the microstructure of the cement paste, the total volume can be considered to be a unit volume. Due to the low content of C_3A, it can be assimilated with C_4AF as V_{AL}. $V_w(t)$ is the remaining water during the hydration reaction, which equals the initial volume of mixed water minus the water consumed during the hydration reactions, equation 16 [43].

$$V_w(t) = V_w^0 - \sum_i V_w^i \times \alpha_i(t) \geq 0 \quad (16)$$

where V_w^0 is the initial water used in the mixture, V_w^i is water consumed for complete hydration of component i, α_i is the hydration rate of component *i*. After total hydration, the volume of remaining water fills the gel pores. V_w^i can be calculated in equations 17 and 18 by using stoichiometric models [43].

$$\frac{V_w^i}{V_c^0} = D_w^i \times \frac{\rho_i'/\mu_i}{\rho_w/\mu_w} \quad (17)$$

$$\rho_i' = \frac{M_i}{V_c^0} = \rho_c \frac{m_i}{\sum_i m_i} \quad (18)$$

where V_c^0 is the initial volume of well cement, $D_w^i = d_w/d_i$, d_w is the moles of consumed water during the hydration reactions, and d_i is the moles of component i consumed during the hydration reactions. ρ_i' is the mass density of different phases. μ_i is the molecular weight. m_i is the mass fraction of different phases of clinker.

The volume changes of the phases in the cement can be calculated using equation 19 [43]. In this study, only the total hydration is considered, and thus the volumes of all initial components in the well cement are reduced to zero.

$$V_{ck}^{i}(t) = V_{ck_0}^{i} \times [1 - \alpha_i(t)] \quad (19)$$

The next step is to calculate the hydration products from the cement. C-S-H gels and calcium hydroxide crystals are produced from C_3S and C_2S. Therefore, equations 20-24 [44] calculate the volume change of the C-S-H gel. The chemical formula used for C-S-H gel is $C_{3.4}S_2H_3$.

$$V_{CSH}(t) = V_{CSH}^{C_3S} \times \alpha_{C_3S}(t) + V_{CSH}^{C_2S} \times \alpha_{C_2S}(t) \quad (20)$$

$$\frac{V_{CSH}^{C_3S}}{V_c^0} = D_{CSH}^{C_3S} \times \frac{\rho'_{C_3S}/\mu_{C_3S}}{\rho_{CSH}/\mu_{CSH}} \quad (21)$$

$$\rho'_{C_3S} = \frac{M_{C_3S}}{V_c^0} = \rho_c \frac{m_{C_3S}}{\sum_i m_i} \quad (22)$$

$$\frac{V_{CSH}^{C_2S}}{V_c^0} = D_{CSH}^{C_2S} \times \frac{\rho'_{C_2S}/\mu_{C_2S}}{\rho_{CSH}/\mu_{CSH}} \quad (23)$$

$$\rho'_{C_2S} = \frac{M_{C_2S}}{V_c^0} = \rho_c \frac{m_{C_2S}}{\sum_i m_i} \quad (24)$$

where $V_{CSH}^{C_3S}$ is the volume of C-S-H gel generated from the C_3S hydration reaction, and $V_{CSH}^{C_2S}$ is the volume of C-S-H gel produced from the C_2S hydration reaction. Similarly, the volume of calcium hydroxide can be obtained through equations 25-27 [44].

$$V_{CH}(t) = V_{CH}^{C_3S} \times \alpha_{C_3S}(t) + V_{CH}^{C_2S} \times \alpha_{C_2S}(t) \quad (25)$$

$$\frac{V_{CH}^{C_3S}}{V_c^0} = D_{CH}^{C_3S} \times \frac{\rho'_{C_3S}/\mu_{C_3S}}{\rho_{CH}/\mu_{CH}} \quad (26)$$

$$\frac{V_{CH}^{C_2S}}{V_c^0} = D_{CH}^{C_2S} \times \frac{\rho'_{C_2S}/\mu_{C_2S}}{\rho_{CH}/\mu_{CH}} \quad (27)$$

The volume of capillary voids can be calculated using the following equation [45].

$$V_{cp} = C_s \times \rho_c \times V_c^0 \times \alpha(t) \quad (28)$$

where C_s is the chemical shrinkage, which equals 0.07 ml/g for regular Portland cement. In this paper, this value is assumed as the chemical shrinkage for Class G cement.

The last step is to calculate the volume fraction of aluminates, which equals the total volume subtracted by all other volume fractions calculated above, shown in equation 29.

$$V_{AL} = 1 - (V_{CSH} + V_{CH} + V_{cp} + V_w + V_{ck}) \quad (29)$$

All the values of parameters mentioned in the equations are summarized in Table 2. It needs to be emphasized that the mass fraction of each clinker phase is decreased during the hydration process with time (C_3S, C_2S, C_3A, C_4AF). On the other side, as the hydration process of the cement proceeds, the mass fraction of CSH and CH is increased.

Table 2 Parameters for determining volume fraction of each phase from cement clinker [46]

	C_3S	C_2S	C_3A	C_4AF	w	c	CSH	CH
Density (g/cm^3)					1	3.15	2.04	2.24
Mass fraction (%)	0.56	0.257	0.02	0.163	-	-	-	-
Molar mass (g/mol)	228.32	172.24	270.2	430.12	18	-	227.2	74
D_{CSH}	1	1	-	-	-	-	-	-
D_{CH}	1.3	0.3	-	-	-	-	-	-
D_W	5.3	4.3	10	10.75	-	-	-	-
Initial volume fraction (%)	-	-	-	-	0.581	0.419	-	-

In addition, from a previous study [46], the volume of water in the gel pores is around 28% of the total volume of the C-S-H gel. Hence, the porosity of C-S-H gel is defined to be 28%. The pore volume in cement paste can be calculated using equation 30.

$$V_{pore} = V_w + V_{cp} + V_{gel} \quad (30)$$

The volume fractions of the components in the cement paste after the completion of the hydration reactions are summarized in Table 3.

Table 3 Volume fraction of the components of the Class G cement after hydration is complete with $w/c = 0.44$

Volume Fraction	%
V_{CH}	18.16
V_{CSH}	57.99
V_W	0.54
V_{cp}	9.24
V_{AL}	14.08

As shown in Table 3, there is not much water left after the total hydration process, which is due to the low water-to-cement ratio used for the cement. The total volume of macro-pores after the cement dries out equals 0.54% + 9.24% = 9.78%. Similar results were obtained by previous studies [47,48].

3 Stoichiometric Model for the Change of Volume Fractions due to the Carbonation Reactions

The initial volume fractions of well cement can be changed during the carbonation reactions. The changes of the volume fractions can be divided into several parts based on the chemical reactions involved, such as degeneration of C-S-H gel, CH crystal, and calcium carbonate. Therefore, the rate of carbonation reaction of each phase needs to be established first, as shown in equation 31 [49].

$$R_i = K_i \times [i] \times [CO_2] \quad (31)$$

where R_i is the rate of carbonation reaction for phase i (C-S-H gel, CH crystal, and calcium carbonate). The rate of reaction describes the generation or degeneration of the phase over time per unit volume. K_i is the coefficient of the carbonation reaction (in unit volume per moles per second), $[i]$ is the concentration of component i (in moles per unit volume of cement), $[CO_2]$ is the concentration of carbon dioxide (in moles per unit volume).

255 The coefficient of the carbonation reaction for C-S-H and CH can be found from TGA
256 experimental results [11]. For a fully saturated condition, $K_{CH}^{0} = 9.9 \times 10^{-3} m^3/mol \cdot s$. In a
257 partially saturated condition, the relationship is shown in equation 32 [49].

258 $$K_{CH} = K_{CH}^{0} \times S^{3.7} \quad (32)$$

259 where S is the saturation level of the cement. S is defined to be 90% of the saturation. The
260 coefficients of the carbonation reaction for C-S-H gel were also developed based on experimental
261 results: $\frac{K_{CSH}}{K_{CH}} = 7.8 \times 10^{-3}$ [49].

262 The concentration of component i is not a constant, but a variable depending on the extent of
263 carbonation reactions, which, in turn, depend on the concentration of CO_2. The concentration of
264 CO_2 is a function of the depth in a structure starting from the boundary, i.e. the surface exposed to
265 CO_2, and the diffusion coefficient of CO_2. It can be calculated with equation 33 [50], which is the
266 solution of the 1D diffusion equation of CO_2 in a large wall.

267 $$C(x,t) = C_s \times (1 - \mathrm{erf}\left(\frac{x}{2\sqrt{Dt}}\right)) \quad (33)$$

268 where C_s is the CO_2 concentration on the boundary of the structure, equaling approximately 0.6-
269 0.8 g/m^3. D is the diffusion coefficient of CO_2, equaling 1.5×10^{-8} to 4.5×10^{-8} m^2/s.
270 After complete hydration of the well cement and initiation of the carbonation reactions, the C-S-
271 H gel and CH crystals degenerates first with infinite moisture and carbon dioxide supply from a
272 leaking borehole system. The production of calcium carbonate fills the capillary voids, which
273 means the generation of calcium carbonate causes the decrease of initial porosity. At the same
274 time, the degeneration of C-S-H gel and CH crystals creates some voids which means the
275 production of calcium carbonate first fills the voids left from the C-S-H gel and CH crystals and
276 then fills the initial capillary voids. In this case, the net effect is a reduction of the porosity. On the
277 other hand, calcium carbonate does not dissolve into the water, but it could react with carbonic

acid to produce bicarbonate. Therefore, the calcium carbonate crystals are further degenerated, and more connected void space appears, which could enable more CO_2 leakage. These changes of porosity are associated with the reactions shown in equations 6 and 7. In this case, the net effect is an increase of the porosity. The rate of increase of the porosity is higher if the reactions shown by equations 6 and 7 are dominant.

The volume of calcium carbonate generated can be divided into two parts. One is produced from the C-S-H gel, the other is produced from the CH crystals. The corresponding equations are:

$$V_{CaCO_3}^{generate}(t) = V_{CaCO_3}^{CSH}(t) + V_{CaCO_3}^{CH}(t) \quad (34)$$

$$V_{CaCO_3}^{CSH}(t) = D_{CaCO_3}^{CSH} \times \frac{\rho_{CSH}/\mu_{CSH}}{\rho_{CaCO_3}/\mu_{CaCO_3}} \times R_{CSH}(t) \quad (35)$$

$$V_{CaCO_3}^{CH}(t) = D_{CaCO_3}^{CH} \times \frac{\rho_{CH}/\mu_{CH}}{\rho_{CaCO_3}/\mu_{CaCO_3}} \times R_{CH}(t) \quad (36)$$

where $V_{CaCO_3}^{CSH}$ is volume of calcium carbonate produced by the C-S-H gel; $V_{CaCO_3}^{CH}$ is the volume of calcium carbonate produced by the CH crystals; $D_{CaCO_3}^{CSH}$ and $D_{CaCO_3}^{CH}$ are proportions of the moles of consumed C-S-H and CH with calcium carbonate during the hydration reactions; ρ is the density; and μ is the molecular weight of each component.

Through the equations above, the processes of calcium carbonate generation, the vanishing of C-S-H gel and CH crystals can be captured clearly. The total amount of calcium carbonate production can also be obtained. The generated calcium carbonate was defined to fill only the capillary pores. This is because the sizes of calcium carbonate crystals are too large to fill the gel pores. In addition, the amorphous silica produced during the reactions can decrease the content of C-S-H gel, which is shown in equation 37.

$$V_{si}^{CSH}(t) = D_{si}^{CSH} \times \frac{\rho_{CSH}/\mu_{CSH}}{\rho_{si}/\mu_{si}} \times R_{CSH}(t) \quad (37)$$

The next step is to calculate the degeneration of calcium carbonate due to the wet carbonation. To simplify the model, the degeneration of the $CaCO_3$ reaction coefficient K is assumed as an average of CH crystals and C-S-H gel. From equation 31, the degeneration rate of $CaCO_3$ can be calculated. To simulate the real situation in a borehole system, the dry carbonation process and the wet carbonation process are assumed to start simultaneously, which means the generated $CaCO_3$ from the dry carbonation process starts to dissolve at the same time

During the carbonation reactions, the net porosity changes can thus be calculated based on the degeneration of C-S-H gel and CH crystals, and the production and degeneration of calcium carbonate. The volume of capillary voids is shown in equations 38-41.

$$V_{cp}(t) = V_{cp}^{0}(t) - [V_{CaCO_3}^{generate}(t) + V_{si}^{CSH}(t) - \Delta V_{CSH}(t) - \Delta V_{CH}(t) - \Delta V_{CaCO_3}(t)] \quad (38)$$

$$\Delta V_{CSH}(t) = V_{CSH} - \sum R_{CSH}(t) \quad (39)$$

$$\Delta V_{CH}(t) = V_{CH} - \sum R_{CH}(t) \quad (40)$$

$$\Delta V_{CaCO_3}(t) = V_{CaCO_3} - \sum R_{CaCO_3}(t) \quad (41)$$

Finally, our calculations show that, during the carbonation reactions, the total volume of cement paste increases, which means there is a volume expansion. The expansion occurs because the volume of the generated calcium carbonate is larger than the reacted C-S-H gel and CH crystals. For convenience, the total volume is normalized to one during the process. All the parameters for the calculation can be found in Table 4.

Table 4 Parameters for determining changes in the volume fraction of cement phases due to the carbonation reaction [46]

	$CaCO_3$	Si
Density (g/cm^3)	2.71	2.04
Molar Mass (g/mol)	100.087	162.6
D_{CSH}	1.7	1
D_{CH}	1	-

As an example, the present theoretical model was used to calculate the impact of carbonation reactions in a 1D 100 cm long well cement sample. The simulation time is for 20 years (7200 days). During this time, the CO_2 is diffused slowly from one side of the sample with high concentration to the other side with low concentration. The calculated CO_2 concentration profile at 20 years, based on equation 33, is shown in Fig. 3. In order to describe the accumulation of CO_2 gas a different depth, the CO_2 concentration at a specific location (20 cm from the concentration head) of the sample for the same timeframe is shown in Fig. 4. The CO_2 concentration at a different depth is shown in Fig. 5. As one can see, for the part of the sample closer to the concentration head, the concentration is much higher.

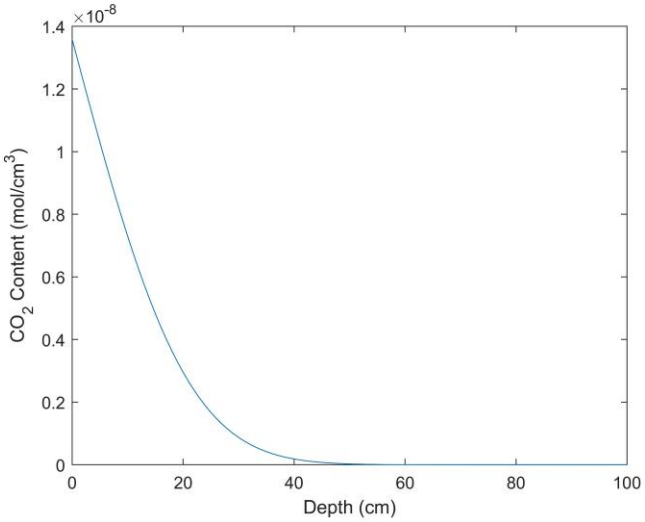

Figure 3. CO_2 profile at 20 years of Class G cement

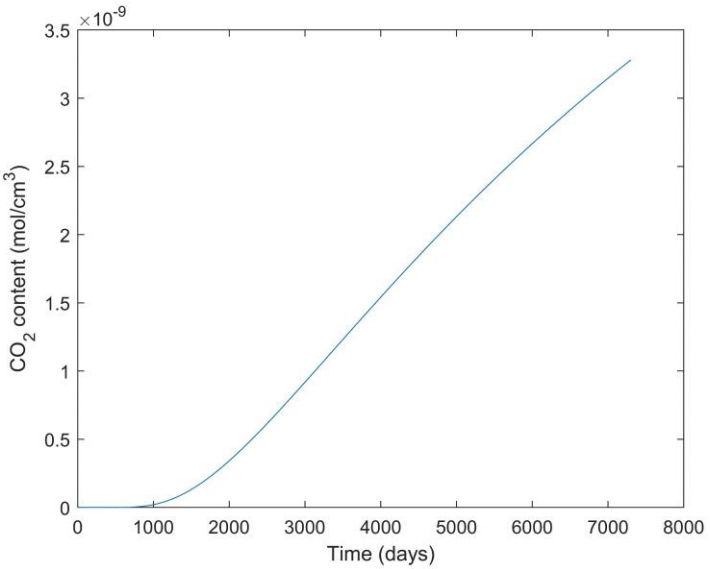

330
331 **Figure 4.** CO_2 content change at 20 years at a 20 cm depth of Class G Cement

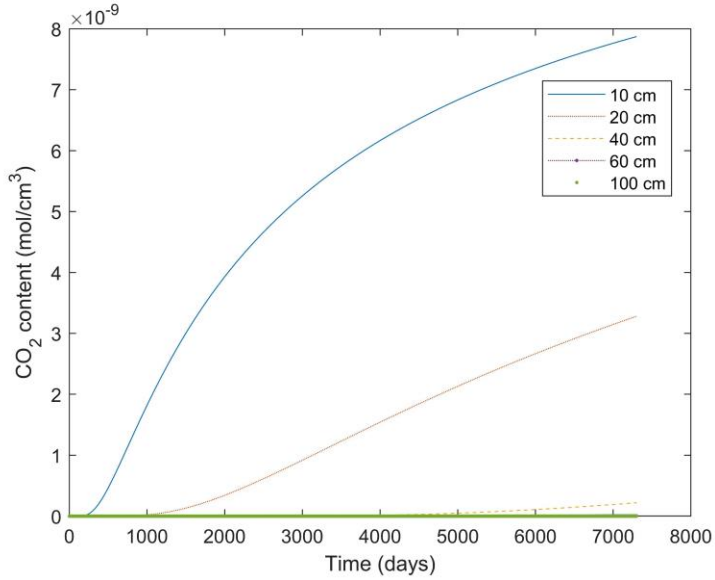

332
333 **Figure 5.** CO_2 content change at 20 years at different depths of Class G cement

334 The results of chemical composition changes are shown in Fig. 6. The volume of calcium carbonate
335 increases in the first eleven years with the dissolution of C-S-H gel and CH crystals. The
336 dissolution of C-S-H is a slow process, while the dissolution of CH is much faster. Since there is
337 unlimited CO_2 and moisture supplied in a leaking borehole, the rate of production of $CaCO_3$ finally
338 becomes lower than the rate of dissolution of $CaCO_3$ due mainly to the major reduction of CH.

This decreases the content of calcium carbonate after 11 years. The CH is completely used up at around 4,200 days, which corresponds to the maximum content of calcium carbonate generated. The volume of C-S-H gel decreases at a much slower rate than the CH crystals because of the low carbonation reaction rate for C-S-H. The amorphous silica, which is produced only from the degeneration of C-S-H, has a small increase which cannot be observed from the figure. In addition, the aluminate phase does not react during the carbonation reactions. Therefore, it maintains a constant volume fraction during the carbonation reactions. However, since the total volume of the sample expands due to the generation of calcium carbonate, the normalized volume fraction of aluminates is slightly decreased. In addition, the chemical composition changes for C-S-H gel, CH crystals, and $CaCO_3$ at different depths are shown in Fig. 7 - Fig. 9. The results showed that the chemical composition change for each phase is highly depended on the concentration of CO_2. With higher concentration of the CO_2 at a shallow depth, the chemical compositions change of Class G cement due to the wet carbonation reaction is faster.

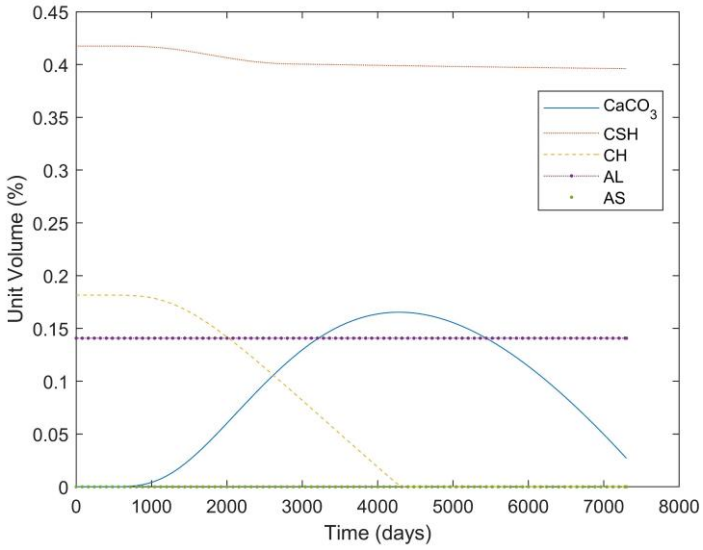

Figure 6. Chemical composition of Class G cement after 20 years of carbonation reaction

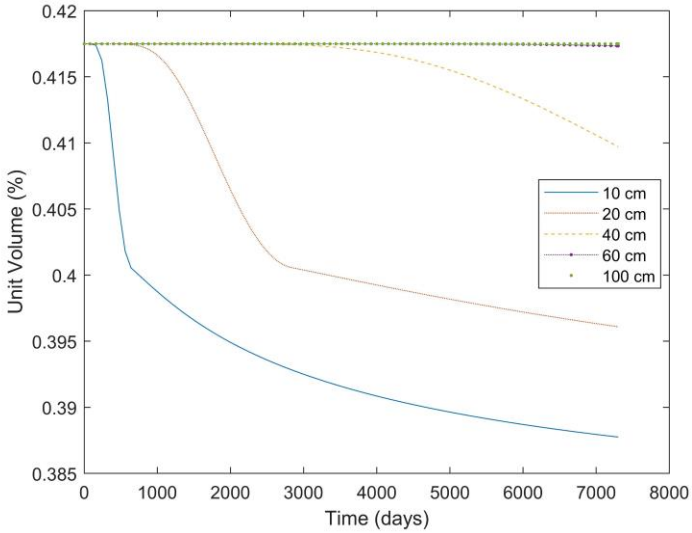

354
355 **Figure 7.** Volume Fraction Change of C-S-H gel after 20 years at different depths

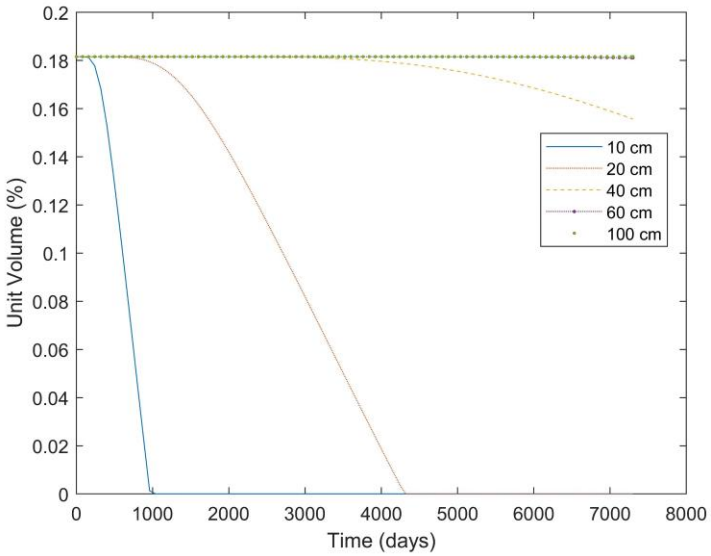

356
357 **Figure 8.** Volume fraction change of CH crystals after 20 years at different depths

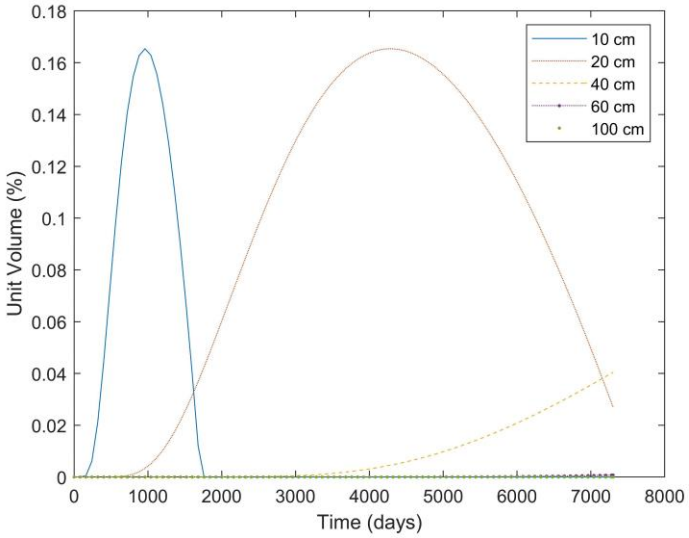

Figure 9. Volume fraction change of $CaCO_3$ after 20 years at different depths

4 The Effect of Carbonation Reactions on the Modulus of Elasticity of Well Cement

Mechanical properties of a composite material depend on its constituent phases. Any change in the volume fractions of the phases results in a variation of mechanical properties of the composite. If a new phase is produced (or an existing phase disappeared) during the service life of a material, the contribution of the phase to mechanical properties of the material must be taken into account. There are many composite mechanics models available that can be used to calculate the effective properties of the composite based on the volume fractions and mechanical properties of the constituent phases [51].

In the present study, a two-phase generalized self-consistent (GSC) model was used for calculating the effective Young's modulus of the carbonated well cement. This model was initially developed for composite materials which include a continuous matrix and spherical pores or rigid inclusions, shown in Fig. 10 [52]. During the carbonation reactions, the changes of the volume fractions of the constituent phases in well cement affected the stiffness of the cementitious material. This process can be modeled by the GSC model. The main equation is:

$$E_{eff} = E_{matrix}\left(1 + \frac{f_{inclusion}}{\left(\frac{1-f_{inclusion}}{3}\right)+\left(\frac{1}{\frac{E_{inclusion}}{E_{matrix}}-1}\right)}\right) \quad (42)$$

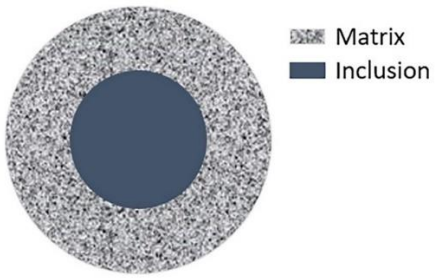

Figure 10. General self-consistant model

This equation shows how to calculate the effective elastic modulus of a two-phase material based on information of the two constituent phases. $f_{inclusion}$ is the volume fraction of the inclusion; $E_{inclusion}$ is the elastic modulus of the inclusion; E_{matrix} is the elastic modulus of the matrix surrounding the inclusion; E_{eff} is the effective elastic modulus of two-phase material, which is the carbonated well cement in the present study.

The Young's moduli of different constituent phases in a carbonated cement are shown in Table 5 [53]. As the amorphous silica is the production of C-S-H gel during the carbonation reaction, shown in equation 4 and 5, it can be assumed that its elastic modulus equals the Young's modulus of C-S-H gel.

Table 5 Elastic modulus of constituents of Class G cement [53]

Compositions	Elastic Modulus (GPa)
C-S-H	22.4
CH	42.3
$CaCO_3$	79.6
Ettringite	22.4
Pores & Voids	0
Amorphous Silica	22.4

In this case, since the carbonated well cement has several phases, equation 42 can be used more than once for each phase. The flow chart for the process is shown in Fig. 11. Specifically, the

process can be split into five steps. As the C-S-H gel and its product, amorphous silica, have the same elastic modulus, they can be merged together and treated as the matrix in the first step, in which, the inclusion phase is the gel pores which are embedded in the C-S-H gel matrix. According to the volume fraction changes of C-S-H and gel pores during the carbonation reactions, equation 42 can be used to calculate the effective Young's modulus of the combination of the two phases. After the effective elastic modulus is calculated for the two phases, in the second step, the combination of C-S-H gel, amorphous silica, and gel pores are considered to be the matrix. The capillary voids in the cement are treated as the inclusion, as shown in the second step in Fig. 10. Then, equation 42 can be used to calculate the new effective elastic modulus of the new combination. In this manner, a new phase can be added into the model step by step until all phases are included. Finally, after using equation 42 five times, all constituent phases can be combined to obtain the general equation for effective elastic modulus of the carbonated well cement at any location of the structure under consideration at any time.

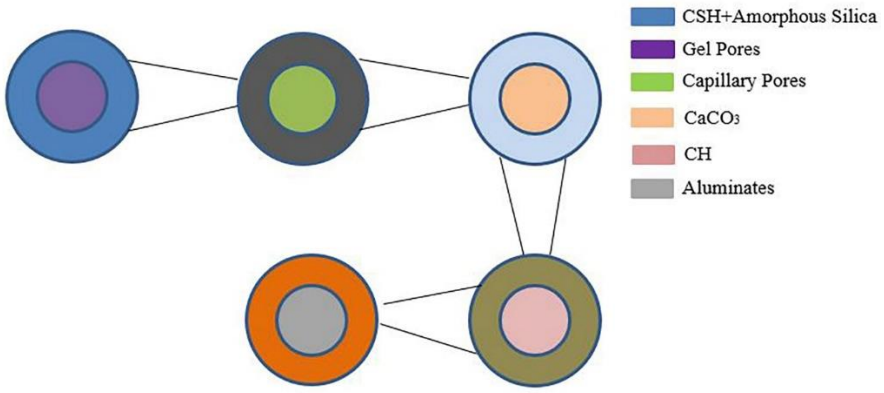

Figure 11. Upscaling method for the cement paste to establish elastic moudlus

This model was used to simulate the elastic modulus of a carbonated well cement at 20 cm, which is shown in Fig. 12 as an example. The result shown in Fig. 12 met our initial expectation that with the continuing intrusion of CO_2, the mechanical properties of cementitious material is decreased

407 due to the degeneration of $CaCO_3$. A similar conclusion has been proven from previous
408 experimental work [54]. Before the carbonation reactions start, the initial Young's modulus after
409 the completion of the hydration reactions is 16 GPa. The dissolution of C-S-H gel and calcium
410 hydroxide causes a decrease of the elastic modulus. At the same time, the generated calcium
411 carbonate from C-S-H gel and CH crystals increases the effective Young's modulus, which offsets
412 the decrease of the elastic modulus. In addition, the production of calcium carbonate dissolves
413 from the beginning of the carbonation reactions. This also causes the drop of the effective elastic
414 modulus. From the figure, it can be seen that the curve can be divided into two parts with the
415 dividing point at the peak value of E_{eff}. In part I (before the peak value), the generation of $CaCO_3$
416 from C-S-H gel and CH crystals is larger than the dissolution of $CaCO_3$ from the wet carbonation.
417 Since the calcium carbonate has a higher elastic modulus than the C-S-H gel and CH crystals, a
418 larger volume fraction of calcium carbonate increases the effective elastic modulus of the well
419 cement. The peak value is around 17.8 GPa at about 3,100 days. In part II (after the peak value),
420 the effective elastic modulus is decreased due to several mechanisms. The governing mechanism
421 is the dissolution of calcium carbonate from the wet carbonation, which is larger in this part than
422 the generation of calcium carbonate from the dry carbonation. Later at about 4,200 days, there is
423 an obvious change of slope in the curve. This point indicates the depletion of CH crystals. Based
424 on the calculation process, the reaction rate of C-S-H gel is much lower than the CH crystals.
425 Therefore, the generation of calcium carbonate in this part is lower, which results in the continuous
426 drop of the effective elastic modulus. After 20 years, the effective elastic modulus of the Class G
427 cement finally drops to 9.6 GPa (the initial value is 16 GPa). In addition, Fig. 13 shows the elastic
428 modulus changes at different depths. As one can see from the result, for a sample at a depth of 10
429 cm, all the carbonation reactions have been completed at around 1,700 days. The remaining elastic

modulus (9 Gpa) is mainly from the ettringite and amorphous silica. For a sample at a depth of 40 cm, the amount of generated $CaCO_3$ is still larger than the amount of $CaCO_3$ dissolved. Therefore, the effective elastic modulus is increased. Besides, for deeper depths: 60 cm and 100 cm, there is almost no concentration of CO_2. Therefore, the elastic modulus does not change since there is no carbonation reaction at those depths.

As mentioned in the introduction section, most of the previous modeling work focused on the dry carbonation (equations 1-5), which happened on the concrete structures above the ground. Therefore, the effective elastic modulus of the cementitious material increased due to the generation of $CaCO_3$. In this case, wet carbonation in the underground environment caused the degeneration of the $CaCO_3$. It means the effective elastic modulus is decreased when the rate of degeneration of $CaCO_3$ is larger than the production of $CaCO_3$. After the long-term process of degeneration of $CaCO_3$ (20 years of simulation time), most of the $CaCO_3$ has been dissolved. The effective elastic modulus is down to 9 Gpa with support only by amorphous silica and aluminates. The carbonated cementitious material has extremely low elastic modulus and leakage is highly possible in the wellbore system. In recent years, several modeling efforts have captured the wet carbonation effect of cementitious materials [55-58]. Compared with these works which focused either on the carbonation depth or the diffusion of calcium ions, this model presents not only the chemical compositions change from stoichiometric model, but also connects directly with the mechanical properties changes by incorporating a general self-consistent model. In addition, the changes of mechanical properties of cementitious material due to the carbonation reaction is commonly measured experimentally, which is restricted by time [59,60]. The reported results in these publications are only in a short-term and cannot represent the real lifetime condition. The predicted results from our modeling work shown in Fig. 12 and 13 are straightforward to be

considered as a reference for estimating the service life of the wellbore due to the carbonation effect.

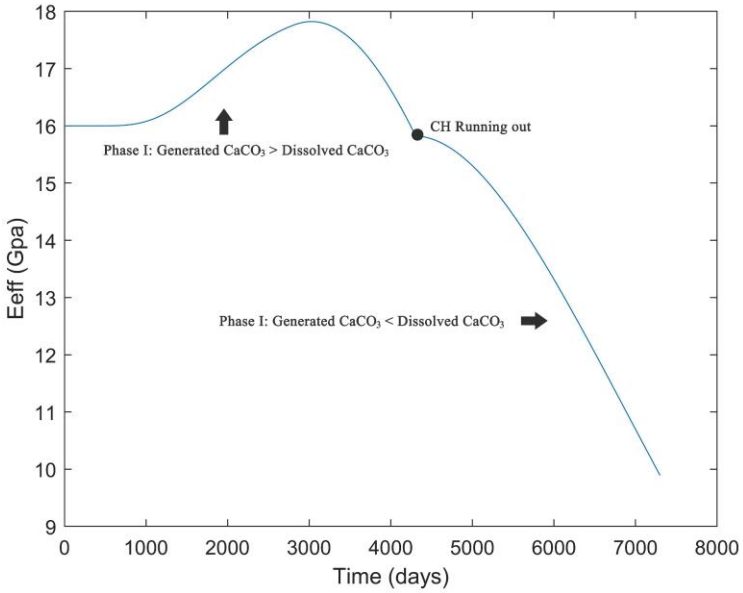

Figure 12. Elastic modulus of Class G cement during the carbonation reaction at a 20 cm depth

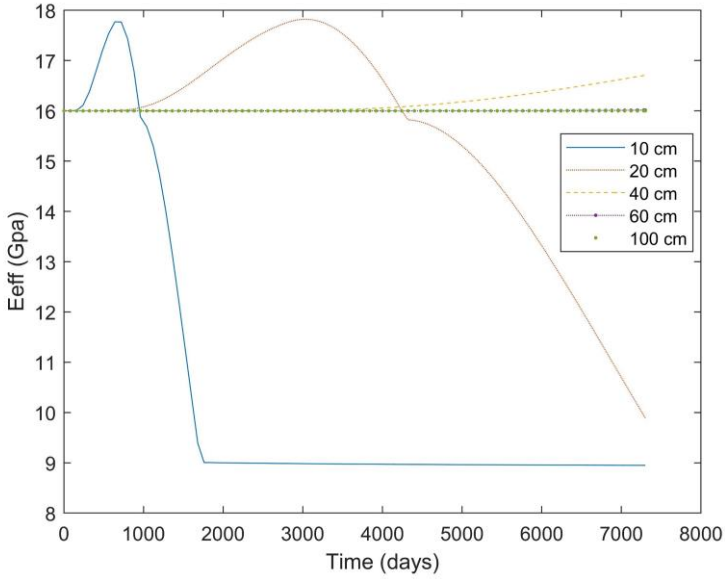

Figure 13. Elastic modulus of Class G cement during the carbonation reaction at different depths

5 Model Validation

To validate the theoretical model, the experimental results from [61] are used to compare with the model prediction. Since there is no experimental data on the carbonation reaction of Class G

cement from previous studies, the tests were conducted using concrete samples made of Type I ordinary Portland cement rather than Class G well cement. Therefore, the fine aggregate and coarse aggregate have to be considered in our model. In the experimental study, three cases with different water-to-cement ratios were used: 0.4, 0.5, and 0.6. The mix design is shown in Table 6. The original chemical composition of Type I cement can be found from ASTM C150. In addition, the elastic modulus of sand and gravel can be found from previous publications [62, 63], which equal 80 GPa and 54 GPa, respectively. All the specimens were cast with dimensions of 10 cm diameter and 20 cm height.

Table 6 Concrete mix design [52]

w/c ratio	Water (kg/m^3)	Cement (kg/m^3)	Sand (kg/m^3)	Gravel (kg/m^3)
0.4	219	548	611	950
0.5	217	434	727	950
0.6	190	317	875	950

After 28 days of curing, the concrete samples were exposed to the air with 1 atm pressure at room temperature and 80% of relative humidity for 21 days. During the test, the elastic moduli of the concrete specimens were tested every 7 days up to 21 days. The material parameters and testing parameters were used as inputs for the theoretical model. It is pointed out that the flow chart shown in Fig. 8 was modified to include the fine aggregate and coarse aggregate for the concrete. Based on the chart for the cement paste as the matrix, the fine aggregate can be included as the inclusions; the effective elastic modulus of the mortar can be calculated. Then the mortar is considered as the matrix, and the coarse aggregate can be included. The carbonation reactions have no impact on the two types of aggregate.

The results of the tests and the theoretical predictions are shown in Fig. 14, Fig. 15, and Fig. 16. From the figures, one can see that the theoretical model can capture the correct trend of the change of elastic modulus of the cementitious material based on the dry carbonation. The dry carbonation

reaction, which is shown in equations 1-5, causes an increase of elastic modulus to the generation of $CaCO_3$. The prediction results showed in the figures are in the reasonable range with acceptable error. The best prediction is for the concrete sample with water-to-cement ratio of 0.5, which provides the closest result compared with the results obtain from experimental study.

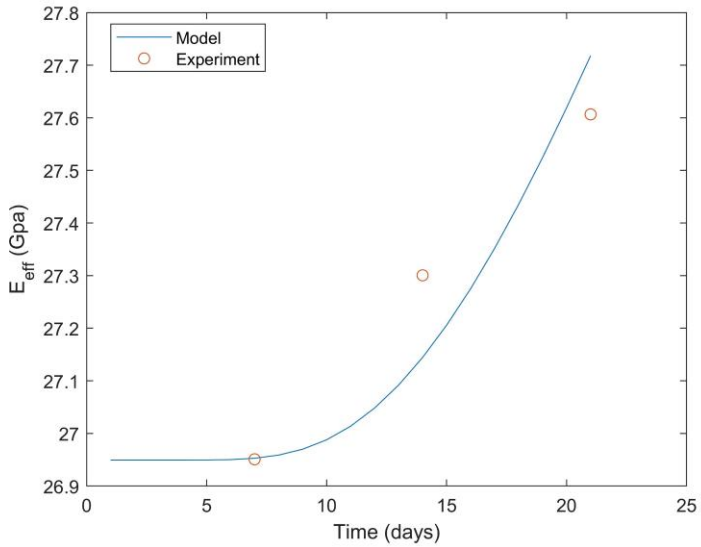

Figure 14. Comparison of model prediction and experimental result with 0.4 w/c concrete sample (Type I Cement)

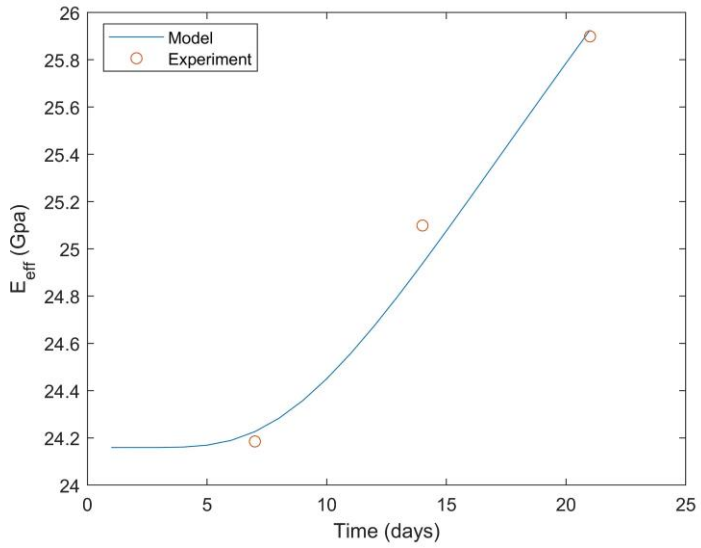

Figure 15. Comparison of model prediction and experimental result with 0.5 w/c concrete sample (Type I Cement)

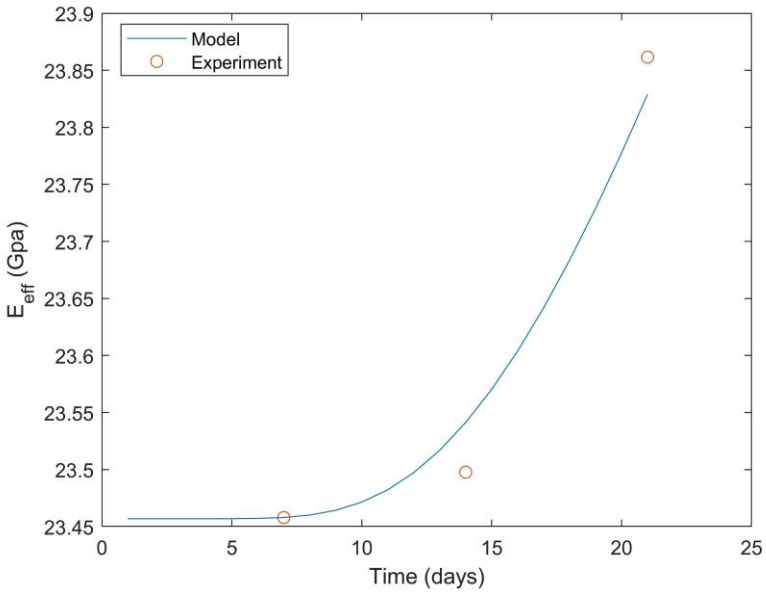

Figure 16. Comparison of model prediction and experimental result with 0.6 w/c concrete sample (Type I Cement)

6 Summary and Conclusions

The underground storage of CO_2 gas has been adopted as one of the most advanced technology for controlling the environmental issue caused by high concentration of CO_2 in the atmosphere. As the main material used for structure of wellbore storage, Class G cement, which is the most used cementitious material in underground CO_2 storage projects due to its low cost and high reliability, provided the stability of the structure and capability of anti-leaking. However, after the long-term performance of a CO_2 underground storage reservoir, the carbonation reactions can cause serious problems to the cementitious material. The changes of chemical composition and mechanical properties of the carbonated cement were characterized by a theoretical model in this study.

(1) The phase transformations of Class G cement during the hydration and carbonation process were predicted by the use of stoichiometric models. The carbonation reactions were assumed to start immediately after the completion of hydration reactions of the cement. Both dry and wet carbonations were considered. The wet carbonation is especially important for the performance of well cement used in underground construction.

(2) The CO_2 profile was predicted by the error function solution of a 1D CO_2 diffusion equation. The CO_2 profile in a cement wall varies with time.

(3) The rate of the carbonation reactions is used in the model. Together with the CO_2 diffusion equation, the CO_2 profile in a cement wall can be predicted accurately. The variations of the volume fractions of the constituent phases in the cement paste due to the carbonation reactions can be calculated using the model.

(4) The generalized self-consistent (GSC) model was used to characterize the changes of mechanical properties during the carbonation reactions. The model can consider the variation of the volume fractions of the constituent phases. The original GSC model was modified to consider more than two phases in the carbonated cement and concrete. Specifically, the effective elastic modulus of well cement was used as a numerical example to show the capacity of the model. The numerical results showed that the carbonation reactions can significantly change the microstructure of well cement and reduce its mechanical properties.

(5) This theoretical model was validated through the comparison with published experimental results of elastic modulus of carbonated concrete. It can predict the change of effective elastic modulus during the carbonation reactions including both dry and wet carbonations.

(6) In conclusion, the modeling work developed in this paper can be used to predict the deterioration of cement annulus in the wellbore system due to the carbonation reaction underground. After the mechanical deterioration of cement annulus, the risk of CO_2 leaking from the wellbore was increased and the potential pollution caused by leaked CO_2 is highly possible. Therefore, the developed model could provide a timeline for controlling the potential environmental problem happened due to the leakage of CO_2 from the underground wellbore. However, calibration work shows that there are some minor differences between model prediction

and experimental results. This is due to the lack of environmental parameters considered in the model, such as the high temperature and high pressure in the wellbore system. In the future, this work could be upgraded by considering the environmental effect, and more accurate results from the model prediction can be achieved.

(7) In addition to the conclusion made above, the minor cracks generated on the well cement due to the carbonation issue is not a severe problem for oil industry application but for CO_2 storage system since it is much more sensitive about the leaking. Based on the results of this study, the current well cement might not be the best cement used for CO_2 storage, a less effective carbonation cement could be developed.

Acknowledgements

Financial support of the U.S. Department of Energy (project Nanoparticle Injection Technology for Remediating Leaks of CO_2 Storage Formation, DE-FE0026514) is gratefully acknowledged.

Data Availability Statement

The raw/processed data required to reproduce these findings cannot be shared at this time as the data also forms part of an ongoing study.

References

[1] G. Moritis, SWP advances CO2 sequestration, ECBM, EOR demos, Oil Gas J. 106 (2008) 60–63.

[2] Y. Shi, K. Jiang, T. Zhang, G. Lv, Cleaner alumina production from coal fly ash: Membrane electrolysis designed for sulfuric acid leachate, J. Clean. Prod. 243 (2020) 118470. doi:https://doi.org/10.1016/j.jclepro.2019.118470.

[3] D. Iribarren, A. Susmozas, F. Petrakopoulou, J. Dufour, Environmental and exergetic evaluation of hydrogen production via lignocellulosic biomass gasification, J. Clean. Prod. 69 (2014) 165–175. doi:https://doi.org/10.1016/j.jclepro.2014.01.068.

[4] R. Nygaard, Well Design and Well Integrity: Wabamun Area CO_2 Sequestration Project (WASP), Energy and Environmental Systems Group, University of Calgary, 2010. http://www.ucalgary.ca/wasp/Well%20Integrity%20Analysis.pdf.

[5] W. Crow, Studies on wellbore integrity, in: the 2nd Wellbore Integrity Network Meeting, Princeton, New Jersey, USA, 28-29 March, 2006.

[6] L. Bertolini, B. Elsener, P. Pedeferri, E. Redaelli, R.B. Polder, Corrosion of Steel in Concrete: Prevention, Diagnosis, Repair, John Wiley & Sons, 2013.

[7] G. Quercia Bianchi, H.J.H. Brouwers, K. Luke, Hydration Kinetics Study of Class G Oil-Well Cement and Olivine Nano-silica Mixtures at 20–60 °C BT - Nanotechnology in Construction, in: K. Sobolev, S.P. Shah (Eds.), Nanotechnol. Constr., Springer International Publishing, Cham, 2015: pp. 179–185. doi:https://doi.org/10.1007/978-3-319-17088-6_22.

[8] A.M. Neville, Properties of Concrete, Prentice Hall, 1995.

[9] L. Li, M.H. Hubler, Y. Xi, Modeling the corrosion of steel casing and the damage of well cement in a borehole system, Constr. Build. Mater. 259 (2020) 119701. doi:https://doi.org/10.1016/j.conbuildmat.2020.119701.

[10] B. Johannesson, P. Utgenannt, Microstructural Changes caused by Carbonation of Cement Mortar, Cem. Concr. Res. 31 (2006) 925-931. doi:https://doi.org/10.1016/S0008-8846(01)00498-7.

[11] V.G. Papadakis, C.G. Vayenas, M.N. Fardis, Experimental investigation and mathematical modeling of the concrete carbonation problem, Chem. Eng. Sci. 46 (1991) 1333–1338. doi:https://doi.org/10.1016/0009-2509(91)85060-B.

[12] A. Rahman, F. Glasser, Comparative Studies of the Carbonation of Hydrated Cements, Adv. Cem. Res. 2 (1989) 49-54. doi:https://doi.org/10.1680/adcr.1989.2.6.49.

[13] Y. Guo, C. Zhao, C. Li, Thermogravimetric Analysis of Carboantion Behaviors of Several Potassium-based Sorbents in Low Concentration CO2, J. Therm. Anal. Calorim. 119 (2015) 441-451. doi:https://doi.org/10.1007/s10973-014-4207-3.

[14] M. Castellote, C. Andrade, Modelling the Carbonation of Cementitious Matrixes by means of the Untreated-Core Model, UR-CORE, Cem. Concr. Res. 38 (2008) 1374-1384. doi:https://doi.org/10.1016/j.cemconres.2008.07.004.

[15] A. Steffens, D. Dinkler, H. Ahrens, Modeling Carbonation for Corrosion Risk Prediction of Concrete Structures, Cem. Concr. Res. 32 (2002) 935-941. doi:https://doi.org/10.1016/S0008-8846(02)00728-7.

[16] B. Bary, A. Sellier, Coupled Moisture-Carbon Dioxide-Calcium Transfer Model for Carbonation of Concrete, Cem. Concr. Res. 34 (2004) 1859-1872. doi:https://doi.org/10.1016/j.cemconres.2004.01.025.

[17] S.-J. Kwon, H.-W. Song, Analysis of Carbonation Behavior in Concrete Using Neural Network Algorithm and Carbonation Modeling, Cem. Concr. Res. 40 (2010) 119-127. doi: https://doi.org/10.1016/j.cemconres.2009.08.022.

[18] L. Jiang, B. Lin, Y. Cai, A Model for Predicting Carbonation of High-Volume Fly Ash Concrete, Cem. Concr. Res. 30 (2000) 699-702. doi:https://doi.org/10.1016/S0008-8846(00)00227-1.

[19] B.G. Kutchko, B.R. Strazisar, G. V Lowry, D.A. Dzombak, N. Thaulow, Rate of CO2 Attack on Hydrated Class H Well Cement under Geologic Sequestration Conditions, Environ. Sci. Technol. 42 (2008) 6237–6242. doi:https://doi.org/10.1021/es800049r.

[20] B.G. Kutchko, B.R. Strazisar, D.A. Dzombak, G. V Lowry, N. Thaulow, Degradation of Well Cement by CO2 under Geologic Sequestration Conditions, Environ. Sci. Technol. 41 (2007) 4787–4792. doi:https://doi.org/10.1021/es062828c.

[21] C. Gervais, A.C. Garrabrants, F. Sanchez, R. Barna, P. Moszkowicz, D.S. Kosson, The effects of carbonation and drying during intermittent leaching on the release of inorganic constituents from a cement-based matrix, Cem. Concr. Res. 34 (2004) 119–131. doi:https://doi.org/10.1016/S0008-8846(03)00248-5.

[22] G. Rimmelé, V. Barlet-Gouédard, O. Porcherie, B. Goffé, F. Brunet, Heterogeneous porosity distribution in Portland cement exposed to CO2-rich fluids, Cem. Concr. Res. 38 (2008) 1038–1048. doi:https://doi.org/10.1016/j.cemconres.2008.03.022.

[23] B. Lecampion, J. Vanzo, F.J. Ulm, B. Huet, C. Germay, I. Khalfallah, J. Dirrenberger, Evolution of Portland Cement Mechanical Properties Exposed to CO2 - Rich Fluids: Investigation at Different Scales, in: Mech. Phys. Porous Solids, 2011: pp. 1–24.

[24] A. Duguid, G.W. Scherer, Degradation of oilwell cement due to exposure to carbonated brine, Int. J. Greenh. Gas Control. 4 (2010) 546–560. doi:https://doi.org/10.1016/j.ijggc.2009.11.001.

[25] D.W.S. Ho, R.K. Lewis, Carbonation of concrete and its prediction, Cem. Concr. Res. 17 (1987) 489–504. doi:https://doi.org/10.1016/0008-8846(87)90012-3.

[26] J. Vanzo, A nanochemomechanical investigation of carbonated cement paste, Massachusetts Institiute of Technology, 2009. http://hdl.handle.net/1721.1/55260.

[27] J. Zhang, E.A. Weissinger, S. Peethamparan, G.W. Scherer, Early hydration and setting of oil well cement, Cem. Concr. Res. 40 (2010) 1023–1033. doi:https://doi.org/10.1016/j.cemconres.2010.03.014.

[28] F. Sajedi, H.A. Razak, Thermal Activation of Ordinary Portland Cement-Slag Mortars. Materials & Design 31 (2010) 4522-4527. doi:https://doi.org/10.1016/j.matdes.2010.04.011.

[29] N.T. Trung, N. Alemi, J.H. Haido, M. Shariati, S. Baradaran, S.T. Yousif, Reduction of Cement Consumption by Producing Smart Green Concretes with Natural Zeolites. Smart Structures and Systems 24 (2019) 415-425. doi:https://doi.org/10.12989/SSS.2019.24.3.415.

[30] M. Shariati, S. Rafiei, P. Mehrabi, Y. Zandi, R. Fooladvand, B. Gharehaghaj, A. Shariati, N.T. Trung, M.N.A. Salih, S. Poi-Ngian, Experimental Invetigation on the Effect of Cementitious Materials on Fresh and Mechanical Properties of Self-Consolidating Conrete. Advances in Concrete Construction 8 (2019) 225-237. doi:https://doi.org/10.12989/acc.2019.8.3.225.

[31] H. Azarijafari, M.J.T. Amiri, A. Ashrafian, H. Rasekh, M.J. Barforooshi, J. Berenjian, Ternary Blended Cement: An Eco-Friendly Alternative to Improve Resistivity of High-Performance Self-Consolidating Concrete Against Elevated Temperature, Journal of Cleaner Production 223 (2019) 575-586. doi:https://doi.org/10.1016/j.jclepro.2019.03.054.

[32] A. Nosrati, Y. Zandi, M. Shariati, K. Khademi, M.D. Aliabad, A. Marto, M.A. Mu\'azu, E. Ghanbari, M.B. Mahdizadeh, A. Shariati, M. Khorami, Portland Cement Structure and Its Major Oxides and Fineness, Smart Structures and Systems 22 (2018) 425-432. doi:https://doi.org/10.12989/sss.2018.22.4.425.

[33] S. Jahandari, M. Saberian, Z. Tao, S.F. Mojtahedi, J. Li, M. Ghasemi, S.S. Rezvani, W. Li, Effects of Saturation Degrees, Freezing-Thawing, and Curing on Geotechnical Properties of Lime and Lime-Cement Concretes, Cold Regions Science and Technology 160 (2019) 242-251. doi:https://doi.org/10.1016/j.coldregions.2019.02.011.

[34] P. Hewlett, M. Liska, Lea's Chemistry of Cement and Concrete, Elsevier Ltd Press, 2003. doi:https://doi.org/10.1016/B978-0-7506-6256-7.X5007-311.

[35] B.G. Kutchko, B.R. Strazisar, D.A. Dzombak, G. V Lowry, N. Thaulow, Degradation of Well Cement by CO2 under Geologic Sequestration Conditions, Environ. Sci. Technol. 41 (2007) 4787–4792. doi:https://doi.org/10.1021/es062828c.

[36] S.D.C. Walsh, H.E. Mason, W.L. Du Frane, S.A. Carroll, Mechanical and hydraulic coupling in cement–caprock interfaces exposed to carbonated brine, Int. J. Greenh. Gas Control. 25 (2014) 109–120. doi:https://doi.org/10.1016/j.ijggc.2014.04.001.

[37] J. Chang, Y. Fang, Quantitative analysis of accelerated carbonation products of the synthetic calcium silicate hydrate (C–S–H) by QXRD and TG/MS, J. Therm. Anal. Calorim. 119 (2015) 57–62. doi:https://doi.org/10.1007/s10973-014-4093-8.

[38] API 10A-11 Specification for Cements and Materials for Well Cementing, American Petroleum Institute Publishing Services, Washington DC, 2002.

662 [39] ASTM C465-18 Standard Specification for Processing Additions for Use in the
663 Manufacture of Hydraulic Cements, ASTM International, West Conshohocken, PA, 2018,
664 https://doi.org/10.1520/C0465-18.

665 [40] ASTM C150/C150M-18 Standard Specification for Portland Cement, ASTM International,
666 West Conshohocken, PA, 2018, https://doi.org/10.1520/C0150_C0150M-18.

667 [41] J.P. Meyer, Summary of carbon dioxide enhanced oil recovery (CO2 EOR) injection well
668 technology, American Petroleum Institute, 2007: pp. 54.

669 [42] M. Bourissai, F. Meftah, N. Brusselle-Dupend, É. Lecolier, G. Bonnet, Evolution of the
670 Elastic Properties of an Oilwell Cement Paste at Very Early Age under Downhole
671 Conditions: Characterization and Modelling, Oil Gas Sci. Technol. – Rev. IFP Energies
672 Nouv. 68 (2013) 595–612. doi:https://doi.org/10.2516/ogst/2012087.

673 [43] O. Bernard, F.-J. Ulm, E. Lemarchand, A multiscale micromechanics-hydration model for
674 the early-age elastic properties of cement-based materials, Cem. Concr. Res. 33 (2003)
675 1293–1309. doi:https://doi.org/10.1016/S0008-8846(03)00039-5.

676 [44] P.D. Tennis, H.M. Jennings, A model for two types of calcium silicate hydrate in the
677 microstructure of Portland cement pastes, Cem. Concr. Res. 30 (2000) 855–863.
678 doi:https://doi.org/10.1016/S0008-8846(00)00257-X.

679 [45] D.P. Bentz, Influence of water-to-cement ratio on hydration kinetics: Simple models based
680 on spatial considerations, Cem. Concr. Res. 36 (2006) 238–244.
681 doi:https://doi.org/10.1016/j.cemconres.2005.04.014.

682 [46] L.E. Copeland, J.C. Hayes, The determination of non-evaporable water in hardened
683 Portland cement paste, ASTM Bull. 194 (1953) 70-74.

684 [47] H.F.W. Taylor, Cement Chemistry, Academic Press, London, 1990.

685 [48] T.C. Hansen, Physical structure of hardened cement paste. A classical approach, Mater.
686 Struct. 19 (1986) 423–436. doi:https://doi.org/10.1007/BF02472146.

687 [49] V.G. Papadakis, C.G. Vayenas, N.F. Michael, Fundamental Modeling and Experimental
688 Investigation of Concrete Carbonation, Mater. J. 88 (1991) 363–373.
689 doi:https://doi.org/10.14359/1863.

690 [50] H. Cui, W. Tang, W. Liu, Z. Dong, F. Xing, Experimental study on effects of CO2
691 concentrations on concrete carbonation and diffusion mechanisms, Constr. Build. Mater. 93
692 (2015) 522–527. doi:https://doi.org/10.1016/j.conbuildmat.2015.06.007.

693 [51] R.M. Christensen, Mechanics of Composite Materials, Wiley Press, New York, 1979.

694 [52] Y. Xi, M. Eskandari-ghadi, A. Suwito, S. Sture, Damage Theory Based on Composite
695 Mechanics, Eng. Mech. 132 (2006) 1195–1204. doi:https://doi.org/10.1061/(ASCE)0733-
696 9399(2006)132:11(1195).

697 [53] C.-J. Haecker, E.J. Garboczi, J.W. Bullard, R.B. Bohn, Z. Sun, S.P. Shah, T. Voigt,
698 Modeling the linear elastic properties of Portland cement paste, Cem. Concr. Res. 35 (2005)
699 1948–1960. doi:https://doi.org/10.1016/j.cemconres.2005.05.001.

700 [54] Y. Yang, B. Yuan, Y. Wang, S. Zhang, L. Zhu, Carbonation resistance cement for CO2
701 storage and injection wells, J. Pet. Sci. Eng. 146 (2016) 883–889.
702 doi:https://doi.org/10.1016/j.petrol.2016.08.006.

703 [55] J. Liaudat, A. Martínez, C.M. López, I. Carol, Modelling acid attack of oilwell cement
704 exposed to carbonated brine, Int. J. Greenh. Gas Control. 68 (2018) 191–202.
705 doi:https://doi.org/10.1016/j.ijggc.2017.11.015.

706 [56] Q.T. Phung, N. Maes, D. Jacques, G. De Schutter, G. Ye, J. Perko, Modelling the
707 carbonation of cement pastes under a CO2 pressure gradient considering both diffusive and
708 convective transport, Constr. Build. Mater. 114 (2016) 333–351.
709 doi:https://doi.org/10.1016/j.conbuildmat.2016.03.191.

710 [57] A. Rezagholilou, V.G. Papadakis, H. Nikraz, Rate of carbonation in cement modified base
711 course material, Constr. Build. Mater. 150 (2017) 646–652.
712 doi:https://doi.org/10.1016/j.conbuildmat.2017.05.226.

713 [58] T. Chen, X. Gao, L. Qin, Mathematical modeling of accelerated carbonation curing of
714 Portland cement paste at early age, Cem. Concr. Res. 120 (2019) 187–197.
715 doi:https://doi.org/10.1016/j.cemconres.2019.03.025.

716 [59] B. Šavija, M. Luković, Carbonation of cement paste: Understanding, challenges, and
717 opportunities, Constr. Build. Mater. 117 (2016) 285–301.
718 doi:https://doi.org/10.1016/j.conbuildmat.2016.04.138.

719 [60] M. Zajac, J. Skibsted, P. Durdzinski, F. Bullerjahn, J. Skocek, M. Ben Haha, Kinetics of
720 enforced carbonation of cement paste, Cem. Concr. Res. 131 (2020) 106013.
721 doi:https://doi.org/10.1016/j.cemconres.2020.106013.

722 [61] J.J. Chang, W. Yeih, R. Huang, J.M. Chi, Mechanical properties of carbonated concrete, J.
723 Chinese Inst. Eng. 26 (2003) 513–522.
724 doi:https://doi.org/10.1080/02533839.2003.9670804.

725 [62] S.-W. Cho, C.-C. Yang, R. Huang, Effect of aggregate volume fraction on the elastic moduli
726 and void ratio of cement-based materials, 2000.

[63] F.P. Zhou, F.D. Lydon, B.I.G. Barr, Effect of coarse aggregate on elastic modulus and compressive strength of high performance concrete, Cem. Concr. Res. 25 (1995) 177–186. doi:https://doi.org/10.1016/0008-8846(94)00125-I.